Fabrication and Properties of an Ultrafast NbN Hot-Electron Single-Photon Detector

Introduction

Currently, visible photon counting is commonplace for advanced optical imaging and spectroscopy. Several types of devices, including photomultiplier tubes,[1] quantum semiconductor avalanche photodiodes,[2] and superconducting tunnel junctions,[3] have been successfully implemented. In general, such detectors work by a cascade mechanism: an incident single photon is absorbed, releasing an electron, which then instigates a multiplication process, leading to a measurable electron current pulse. Unfortunately, vacuum photomultipliers are slow and bulky and have an extremely low quantum efficiency for longer-wavelength photons. The major drawback of the most popular and most successful silicon photodiodes is that the wavelength sensitivity is limited to below 1 μm, restricted by the Si bandgap. In addition, the single-photon avalanche photodiodes exhibit low detection rates due to complicated Geiger-mode readout schemes.

The current most-pressing need is to develop practical infrared single-photon detectors, operational at either 1.3 μm or 1.55 μm, for novel quantum communication and quantum computation systems. The problem is that infrared photons carry significantly less energy than those of visible light, so in this case it is difficult to engineer an efficient electron cascade mechanism. Avalanche photodiodes based on narrow-gap semiconducting materials exhibit unacceptably large dark counts, while recently proposed single-electron transistors[4] are slow and require millikelvin temperatures and tesla-level magnetic fields.

In this article, we present a simple-to-manufacture and easy-to-operate, NbN hot-electron photodetector (HEP) with picosecond response time, high intrinsic quantum efficiency, negligible dark counts, and the capability to detect single photons from the ultraviolet to the infrared wavelength range. Our photodetector is the conversion of a well-known, unselective, superconducting hot-electron bolometer[5] into an optical and infrared wavebands quantum detector.[6] The detector consists of an ultrathin, submicron-width NbN stripe, maintained at 4.2 K and current-biased close to the critical value. The detection mechanism is based on supercurrent-assisted, temporary formation of a resistive barrier across the stripe due to photon-induced hot-spot generation. Practical implementation of this device should lead to revolutionary progress in areas ranging from ultrafast free-space satellite communication[7] through quantum computation[8] and quantum cryptography[9] to semiconductor integrated circuit testing.[10]

Device Fabrication

NbN films were sputtered onto sapphire substrates by reactive magnetron sputtering in an argon–nitrogen gas mixture. Using an optimized sputtering technique, the NbN samples exhibited a superconducting transition temperature of T_c = 10.5 K for 60-Å-thick films and 11 K for 100-Å-thick films, respectively. The superconducting transition width was equal to ΔT_c = 0.3 K. A more detailed description of the NbN film deposition can be found in Ref. 11.

The fabrication process of the HEP's included several deposition and patterning manufacturing stages, resulting in the devices shown in Figs. 85.35 and 85.36. After the NbN film sputtering, TiAu alignment marks for future lithography steps and interior 5-μm × 16-μm Ti/Au contacts were formed using *e*-beam lithography and *e*-beam evaporation. Exterior contact pads for wire bonding of the entire structure were fabricated by a vacuum evaporation of 2000 Å of Au. The final, desired geometry of the NbN microbridge was achieved by ion milling the NbN film through a 200-Å-thick Ti mask placed inside the gap between the inner Ti/Au contacts. For a straight bridge (Fig. 85.35) this mask was a single 0.2-μm-wide stripe, while in the case shown in Fig. 85.36, it was a 0.2-μm-wide meander-type line covering the 4-μm × 4-μm area. After ion milling of the NbN detector, the remaining Ti layer was chemically removed.

After fabrication, each device was carefully inspected using both the AFM (Fig. 85.35) and SEM (Fig. 85.36) microscopes for bridge uniformity. In addition, the only samples selected were those in which room-temperature resistance was almost equal to the value calculated according to the structure dimen-

sions and measured sheet resistance of the unpatterned NbN film. This procedure assured homogeneity and high quality of the superconductor microbridge, with minimal, if any, variations along its width.

Experimental Setup

The experimental setup and device connections inside an optical liquid-helium cryostat are shown schematically in Fig. 85.37. The NbN HEP was mounted on a cold plate and maintained at $T = 4.2$ K. Two cold glass filters were used to prevent the room-temperature thermal radiation from falling onto the device. The device was mounted on a rigid coplanar transmission line and connected with a cold bias-tee through a stainless steel, semirigid coaxial cable. The ac output of the bias-tee was connected to a cryogenic low-noise amplifier. Outside the dewar, the signal passed through a second power

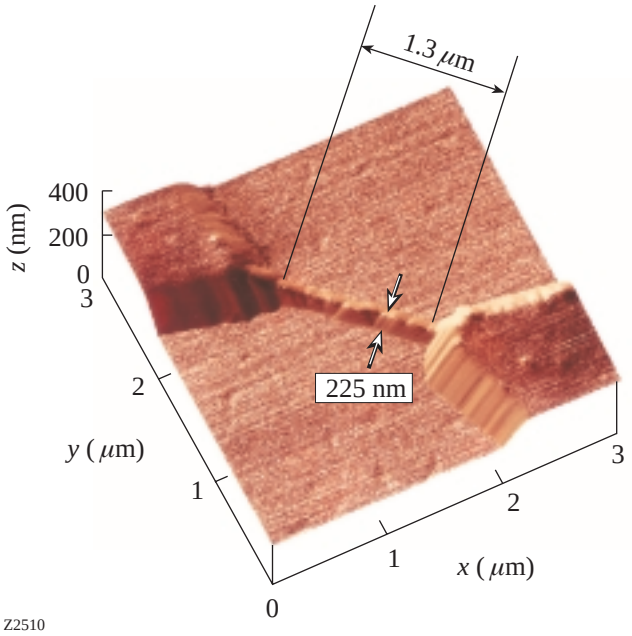

Figure 85.35
AFM image of a 1.3-μm × 0.23-μm simple bridge device.

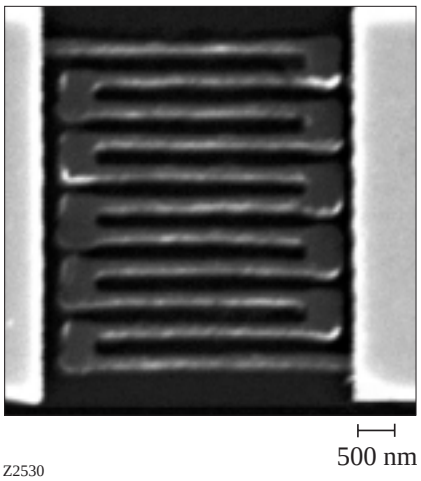

Figure 85.36
SEM photograph of a meander-type photodetector structure.

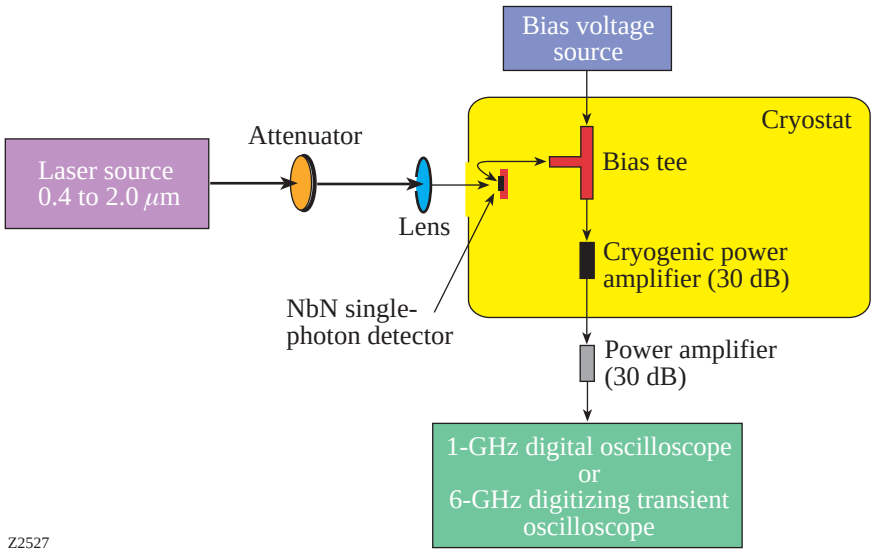

Figure 85.37
Experimental setup.

amplifier, connected to a single-shot oscilloscope and pulse counter (not shown). The oscilloscope was either externally triggered by laser pulses or self-triggered. The experiments were performed using 20-ps-wide, ~3-pJ-energy, 0.85-μm-wavelength pulses generated by a GaAs laser with a repetition rate ranging from 1 Hz to 100 kHz, or 100-fs-wide optical pulses from a mode-locked Ti:sapphire laser. In this latter case, the wavelength could be varied quasi-continuously from 0.5 μm to 2.1 μm, while the repetition rate was either 76 MHz or 1 kHz. The intensity of the laser pulses was attenuated using banks of neutral-density filters. The diameter of the beam incident on the device was always at least 200 μm, assuring stable (no "beam walking") and uniform illumination throughout the experimental session.

Experimental Results

An experimental *I-V* curve for meander-type HEP, measured by a two-point method, is presented in Fig. 85.38. The curve is typical for a long superconducting microbridge and shows that depending on the biasing condition (either purely current-bias or voltage-bias), the device switches from the superconducting, zero-resistance state to the switched, resistive state. This particular device exhibits $I_c = 80$ μA and the switched-state resistance $R = 46$ kΩ. The dashed line between points A and B in Fig. 85.38 represents the switching condition when the device is connected to a 50-Ω microwave transmission line. For a HEP biased close but below I_c (point A in Fig. 85.38), the photon absorption leads to a temporary switch along the dashed line to the metastable resistive point B. As a result, a voltage pulse is observed whose amplitude corresponds to the voltage value of point B, while the duration depends on the dynamics of formation and destruction of the resistive state induced by the photon absorption (see the **Discussion** section).

The time-resolved HEP response to a 0.85-μm-wavelength, 20-ps-wide optical pulse, captured using a single-shot, 6-GHz-bandwidth digitizing oscilloscope, is shown in Fig. 85.39. The width of the photoresponse is equal to ~150 ps and, based on our earlier electro-optic time-domain measurements,[12] is limited by the upper cutoff frequency of our amplifier chain. The signal-to-noise ratio is ~30 dB. Qualitatively, the same response pulses, with the same ~150-ps pulse widths and essentially the same amplitudes, were obtained at all the studied photon energies, independently of the incident optical pulse width, or the laser repetition rate. In addition, the response amplitude did not depend on the laser beam intensity.

Device Operation

Figure 85.39 shows the quantum nature of the HEP detector, but it does not show indisputably that it is indeed a single-photon counter. To demonstrate the latter, the statistical dependence of the number of recorded photoresponse pulses on the number of input quanta per pulse per unit area was measured. We progressively attenuated the intensity of laser pulses, using calibrated neutral density filters, and observed the decreasing number of response pulses. The experimental data allowed us to calculate the probability of recording a detector output for a given photon flux input, which is shown in Fig. 85.40 for two different device types. Curves *a* and *b* correspond to a simple,

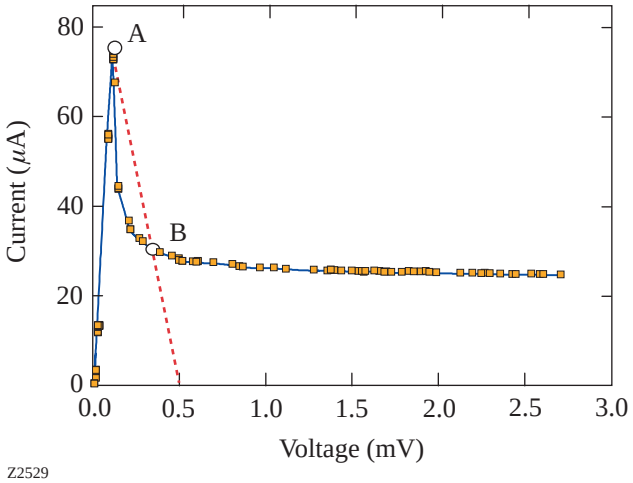

Figure 85.38
I-V curve of a meander-type device measured at $T = 4.2$ K.

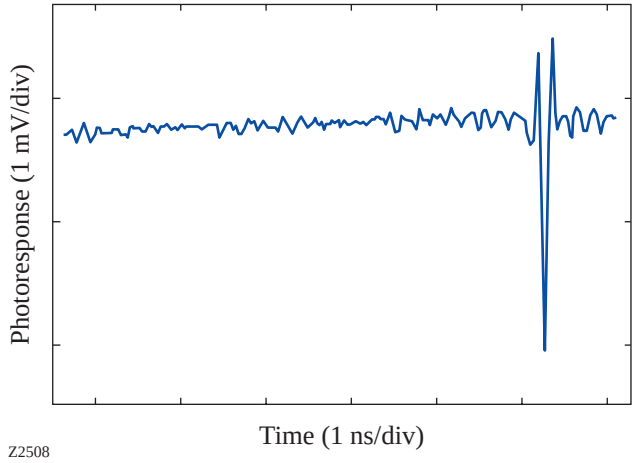

Figure 85.39
Time-resolved, single-photon-type event recorded by a single-shot digitizing oscilloscope.

1-μm-long microbridge, biased at the current value $I_b = 0.92\, I_c$ and $I_b = 0.8\, I_c$, respectively. Curves *c* and *d* are taken for a meander-type device, under the same conditions as curves *a* and *b*, respectively.

Note that while for high photon fluxes both HEP's are saturated, showing 100% efficiency in photon counting, the significant decrease in the number of photons *m* per pulse results in lower probability of recording a photon. Based on simple statistics, one can expect that for very weak photon fluxes, the probability of detecting one photon should be proportional to *m*, while the probability of simultaneously detecting two photons depends on m^2, the three-photon counting should obey the m^3 law, and so on. Indeed, we observe the linear decrease of response pulse probability versus number of quanta per unit area for curves *a* and *c*. At the same time, curve *b* follows a clear m^2 dependence, indicating a two-photon detection. Thus, the 0.92 ratio of I_{bias}/I_c is required for the single-photon operation. In general, photon detection probability versus I_{bias} was an exponentially decreasing function, indicating that the I_{bias} redistribution from the uniform state to the sidewalk-restricted flow, rather than the hot-spot formation, is the dominant factor of the device response.

The other characteristic parameter of a single-photon detector is its quantum efficiency, defined as the ratio of the number of response pulses to the number of incident photons per area for the device in the linear regime (Fig. 85.40, curves *a* and *c*). The quantum efficiency for the microbridge (curve *a*) may be estimated as 20%. The meander-type HEP's have been designed to increase both the active area of the device and its total quantum efficiency. As was expected, the absolute quantum efficiency for the meander device is significantly higher than that for the 1-μm device, but the detector's active area was increased by the factor of 80, while the quantum efficiency increased only 20 times. Thus, the intrinsic quantum efficiency for the meander HEP is equal to approximately 5%. The reason for the observed decrease in the meander device's performance might be associated with the limited uniformity of the device width over the very long length of the meander stripe. We also note that in the case of the lower bias current (Fig. 85.40, curve *b*), the meander device exhibits a nonlinear probability dependence on the photon flux.

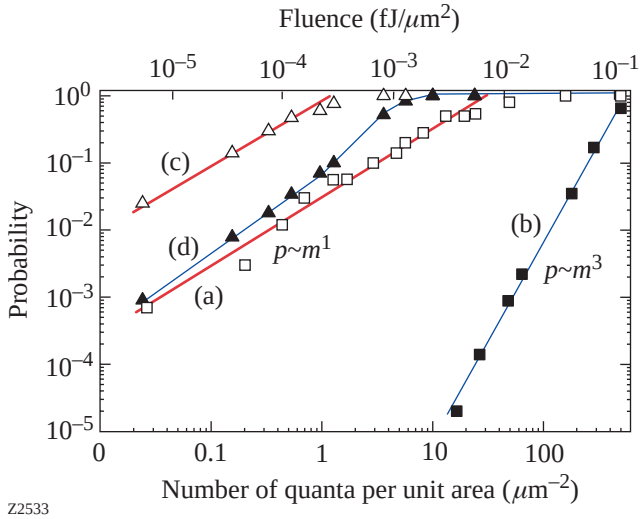

Figure 85.40
Dependence of the detector response probability on the number of incident photons per pulse per unit area. Curves *a* and *b*: microbridge-type device; curves *c* and *d*: meander-type device; △, □: $I_b = 0.92\, I_c$; ▲, ■: $I_b = 0.8\, I_c$.

Discussion and Conclusions

The physical mechanism of operation of the NbN HEP optical single-photon counter is based on supercurrent-assisted, temporary formation of a resistive barrier across the stripe due to photon-induced hot-spot generation and is presented in Ref. 13. A single optical photon is absorbed by an ultrathin, very narrow stripe of a NbN superconductor, maintained at a temperature well below T_c, and biased with I_{bias} close to the device I_c. The photon absorption generates a very high number of excited, hot electrons, leading to local suppression of superconductivity and hot-spot formation. The resistive hot spot pushes the supercurrent out of the center of the stripe, causing it to exceed the critical value for the remaining superconducting part, and leading to the formation of a resistive barrier across the entire width of the device. For the current-biased sample, this resistance results in a large, easily measurable voltage signal. The subsequent hot-electron outdiffusion and cooling lead to hot-spot healing and the collapse of the resistive barrier. The superconductivity is restored in approximately 30 ps,[12] and the detector is ready to register another photon.

The main difference between our detection mechanism and the earlier proposed hot-spot mechanism[14] is that our response is due to a collaborative effect of the bias current and the radiation quantum, leading to a large voltage output signal. To a certain extent the magnitude of the voltage pulse does not depend on the quantum energy, although the pulse shape does, providing the basis for the spectral sensitivity of the device. The rate of photon counting, which can be defined as the inverse of the total photon response time, is also a direct function of the operating parameters and can be as fast as tens

of gigahertz. Finally, as we have demonstrated, depending on the device's operating parameters, our HEP can act as a single-photon, two-photon, or even three-photon quantum counter.

Our device should be able to find immediate applications, primarily in the area of ultrafast near-infrared photon counting, where there are currently no competing technologies. The 1.3-μm- to 1.55-μm-wavelength range is important for optical communication. Already-identified applications of our superconducting HEP's range from sensing ultraweak electroluminescence from submicron complementary metal-oxide-semiconductor VLSI circuits to quantum cryptography and quantum computation.

ACKNOWLEDGMENT

We wish to thank Kenneth Wilsher and Steven Kasapi for helpful discussions.

REFERENCES

1. Photomultiplier tubes, Hamamatsu Photonics K.K., http://www.hamamatsu.com (2000).
2. F. Zappa *et al.*, Opt. Eng. **35**, 938 (1996).
3. A. Peacock *et al.*, Nature **381**, 135 (1996); R. J. Schoelkopf *et al.*, IEEE Trans. Appl. Supercond. **9**, 293 (1999).
4. S. Komiyama *et al.*, Nature **403**, 405 (2000).
5. G. N. Gol'tsman, Infrared Phys. Technol. **40**, 199 (1999).
6. K. S. Il'in *et al.*, Appl. Phys. Lett. **73**, 3938 (1998).
7. G. G. Ortiz, J. V. Sandusky, and A. Biswas, in *Free-Space Laser Communication Technologies XII*, edited by G. S. Mercherle (SPIE, Bellingham, WA, 2000), Vol. 3932, pp. 127–138.
8. E. Knill, R. Laflamme, and G. Milburn, "Efficient Linear Optics Quantum Computation," (http://arXiv.org/abs/quant-ph/0006088) (2000).
9. G. Gilbert and M. Hamrick, "Practical Quantum Cryptography: A Comprehensive Analysis (Part One)," *MITRE Technical Report*, Report No. MTR 00W0000052 (http://xxx.lanl.gov/abs/quant-ph/0009027) (2000); to appear in Physics Reports.
10. J. C. Tsang and J. A. Kash, Appl. Phys. Lett. **70**, 889 (1997).
11. S. Cherednichenko *et al.*, in *Proceedings of the Eighth International Symposium on Space Terahertz Technology* (Harvard University, Cambridge, MA, 1997), pp. 245–252.
12. K. S. Il'in, M. Lindgren, M. Currie, A. D. Semenov, G. N. Gol'tsman, R. Sobolewski, S. I. Cherednichenko, and E. M. Gershenzon, Appl. Phys. Lett. **76**, 2752 (2000).
13. G. N. Gol'tsman, O. Okunev, G. Chulkova, A. Lipatov, A. Semenov, K. Smirnov, B. Voronov, A. Dzardanov, C. Williams, and R. Sobolewski, "Picosecond Superconducting Single-Photon Optical Detector," submitted to Applied Physics Letters.
14. A. M. Kadin and M. W. Johnson, Appl. Phys. Lett. **69**, 3938 (1996).